DOI: 10.26599/FSHW.2026.9251020

Contents lists available at SciOpen

Food Science and Human Wellness

journal homepage: https://www.sciopen.com/journal/2097-0765

China Food Publishing Co.

Diallyl Trisulfide Suppresses 4-(Methylnitrosamino)-1-(3-pyridyl)-1-butanone-Induced Lung Carcinogenesis via Modulating Keap1-Nrf2 Axis

Jiarui Ding [a,1], Tianyuan Wang [a,1], Rui Chen[a], Lei Zhang [b], Wenli Zhao [c], Muqi Li [a], Zhuo Qu [a*]

[a] *Key Laboratory of Protection, Development and Utilization of Medicinal Resources in Liupanshan Area, Ministry of Education, College of Pharmacy, Ningxia Medical University, 1160 Shengli Street, Yinchuan, Ningxia 750004, China*

[b] *Department of Pharmacy, The First People's Hospital of Yinchuan, 2 Liqun Street, Yinchuan, Ningxia, 750000, China*

[c] *Department of Pharmacy, General Hospital of Ningxia Medical University, 804 Shengli Street, Yinchuan, Ningxia 750003, China*

ABSTRACT: Smoking remains strongly associated with lung cancer, underscoring the need for effective chemopreventive strategies derived from dietary sources. This study is focused on the protective effects of diallyl trisulfide (DATS) against 4-(methylnitrosamino)-1-(3-pyridyl)-1-butanone (NNK) triggers lung tumor formation. DATS is a bioactive organosulfur compound sourced from garlic. In an A/J mouse model, DATS administration significantly reduced lung tumor multiplicity. In vitro assays using MRC-5 human lung fibroblasts demonstrated that DATS mitigated NNK-induced cytotoxicity. Mechanistic studies indicated that DATS-mediated Nrf2 pathway activation, via Keap1 dissociation and nuclear translocation, upregulates antioxidant defense genes. Critically, pharmacological inhibition of Nrf2 abolished the protective effects of DATS, pointing to the pathway as central to the effect. Our results position DATS as a promising candidate for dietary prevention of lung cancer. Taken together, this study suggests that DATS has promise as a dietary strategy to prevent lung cancer.

Keywords: Diallyl disulfide, Lung cancer, Keap1-Nrf2 axis, 4-(methylnitrosamino)-1-(3-pyridyl)-1-butanone, Food functions, Chemoprevention

1. Introduction

As the foremost cause of cancer-related mortality globally, approximately 1.8 million annual deaths worldwide, lung cancer presents a particularly severe challenge in China, where its incidence and mortality lead all other malignancies[1-3]. Long-term survival rates for lung cancer patients are unsatisfactory, usually less than 20%, primarily attributed to limitations in reliable early detection methods and effective therapeutic options [4]. Established risk factors include tobacco use, environmental pollution, and occupational exposures [5], with epidemiological evidence indicating that smoking and associated carcinogens contribute to approximately 90% of cases [6]. Smoking cessation represents the most effective evidence-based prevention strategy. Nevertheless, challenges in sustained cessation adherence perpetuate tobacco-related lung cancer as a significant public health burden. Of note, Nature News 2022 highlights in the form of a title that nearly 50%

[1] These authors contributed equally.
***Corresponding author**
Email address: quzhuo2008@163.com (Z. Qu).

Received 20 October 2025
Received in revised from 28 November 2025
Accepted 24 February 2026

of cancers are preventable [7]. Preventing smoking-induced lung cancer is crucial for reducing its incidence and improving patient survival rates, while providing better prognoses through early detection and treatment. Consequently, developing targeted preventive and therapeutic strategies addressing definitive etiological factors and key pathogenic mechanisms is critical for effective lung cancer control [8].

The World Health Organization (WHO) identifies bring into contact with cigarette smoke as a serious public health threat that not only affects active smokers but also poses significant health risks to passive smokers. In addition to this broad risk, tobacco smoke harbors more than 60 known carcinogens, among which 4-(methylnitrosamino)-1-(3-pyridyl)-1-butanone (NNK) is a particularly potent carcinogen, underscoring its severe health implications [9, 10]. Experimental evidence confirms the tumorigenicity of NNK across multiple species, establishing its role as a human lung carcinogen [1]. Notably, NNK induces lung adenomas and adenocarcinomas in multiple species, with A/J mice being particularly susceptible due to their heightened sensitivity to development of lung tumors [11]. The activation of NNK metabolite 4-(methyl)-N-methyl-N-(methyl)-N-nitrosamino)-1-(3-pyridyl)-1-butanol (NNAL) through CYP450-mediated processes to form DNA adducts is a crucial mechanism step. Unrepaired or misrepaired adducts can cause genetic mutations that contribute to tobacco-induced lung carcinogenesis [12].

Inducing phase II detoxifying enzymes is a well-established strategy for effectively preventing experimental carcinogenesis in rodents [13]. Carcinogenesis is often driven by oxidative stress—a state of imbalance where an excess of reactive oxygen species (ROS) overwhelms the cellular antioxidant defenses, resulting in oxidative damage [14]. Acting as a master regulator, the nuclear factor-erythroid-2-related factor 2 (Nrf2) regulates a network of cytoprotective genes—including detoxifying proteins and antioxidant such as quinone oxidoreductase 1 (NQO1) and heme oxygenase-1 (HO-1)—making its pathway a key target for chemoprevention against oxidative damage [13, 15]. Electrophilic or oxidative stress triggers the dissociation of Nrf2 from its inhibitor, Keap1. The liberated Nrf2 then translocates into the nucleus to activate transcription via antioxidant response elements (AREs) [16]. This activation of the Nrf2 pathway upregulates the oxidative stress protection system, mitigates inflammation, and reduces apoptosis. Consequently, the Nrf2-mediated adaptive response constitutes a vital protective mechanism against lung tumorigenesis [13, 17-19], underpinning the efficacy of chemopreventive agents that target this pathway.

Accumulating evidence indicates that dietary factors significantly contribute to cancer risk reduction, with numerous foods, beverages, and bioactive constituents demonstrating efficacy in lung cancer chemoprevention and adjuvant therapy [20-22]. Among natural products with promising chemopreventive properties, *Piper methysticum* (kava), a traditional South Pacific food supplement, exhibits notable the chemopreventive effect on lung cancer. Studies have identified dihydromethysticin (DHM) as a key bioactive kava constituent capable of blocking lung tumor formation induced by cigarette carcinogens in A/J mice, with crude kava extracts similarly suppressing NNK-induced pulmonary carcinogenesis [23-28]. *Houttuynia cordata* (fishwort), a pharmacopeial herb in China, exerts chemopreventive effects against benzopyrene (BaP)-induced lung tumors through activation of the Nrf2-HO-1/NQO1 pathway[13]. Bioactive organosulfur

compounds, including diallyl disulfide (DADS) and diallyl trisulfide (DATS), are found in garlic (*Allium sativum*), one of the oldest and most important herbs [29]. The health benefits of these garlic compounds include the inhibition of neoplastic growth, achieved by triggering anti-inflammatory and antioxidant responses [30]. We previously showed that garlic oil suppresses NNK-mediated injury in both A/J mice and MRC-5 cells, mediated through changes in phase II enzyme expression [31]. DADS exhibits broad-spectrum organoprotection and anticancer activity via antioxidative and/or anti-inflammatory mechanism [32], with our prior work crucially establishing its suppression of NNK-driven lung tumorigenesis through Nrf2 activation and NF-κB inhibition [33]. DATS not only attenuated cisplatin-induced oxidative damage in patients by enhancing antioxidant capacity but also protected against NNK- triggered lung injury in A/J mice by altering intestinal flora and inhibiting NF-κB [34, 35]. Building upon this foundation, the present study specifically investigates the chemopreventive efficacy of DATS against lung tumorigenesis triggered by NNK, elucidates the role of oxidative stress mitigation in its mechanism, and functionally validates Nrf2 pathway activation.

2. Materials and methods

2.1 Chemicals, reagents, and animal diets

DATS and the tobacco-specific nitrosamine NNK (**Fig. 1A**) were acquired from Sigma-Aldrich. AIN-93G and AIN-93M purified diets were supplied by Beijing Ke'ao Co-operative Feed Co., Ltd. The primary antibodies used were anti-Nrf2 (1:1000, Proteintech, Wuhan Sanying, Hubei, China; 1:2000, Biodragon, Suzhou Biodragon, China; 1:1000, Abcam, America), anti-HO-1 antibody (1:1000, Proteintech, Wuhan Sanying, Hubei, China), anti-NQO1 (1:1000. Proteintech, Wuhan Sanying, Hubei, China), anti-Keap1 antibody (1:2000, Proteintech, Wuhan Three Eagles, Hubei, China), anti-GAPDH (1:5000, Proteintech, Wuhan Three Eagles, Hubei, China), anti-Beta-actin (1:10,000, Proteintech, Wuhan Three Eagles, Hubei, China), and goat anti-rabbit IgG (1:5000, Proteintech, Wuhan Sanying, Hubei, China). We ordered all primers from Sangon Biotech Co., Ltd (Shanghai, China).

2.2 Animals and treatments

Female A/J mice (5-6 weeks old, SPF) from The Jackson Laboratory were housed in the Laboratory Animal Center of Ningxia Medical University. Mice were maintained at a constant temperature of 23 ± 1 °C, 50% humidity, and a 12 h light/dark cycle, with food and water provided ad libitum. All procedures involving animals were in accordance with the National Guidelines for the Management and Use of Laboratory Animals (Guidelines for Ethical Review of Laboratory Animals for Animal Welfare in China) (GB/T358922018) and authorized by the Animal Management and Use Committee of Ningxia Medical University (Certificate No. 2022-N123). After one week of mouse rearing, the mice were randomly divided into a control group, an NNK model group, and a DATS treatment group, with 12 mice in each group. Concurrent with the start of the experiment, the DATS group began daily gavage of 23 mg/kg DATS in 0.5% carboxymethylcellulose sodium (CMC-Na), with control and NNK groups receiving the vehicle. This was followed one week later with a single i.p. injection of NNK (100 mg/kg) to the NNK and DATS groups, whereas the control group was

administered saline. The animals were fed the high-energy AIN-93G diet for the first 21 days to support juvenile growth, followed by the standard AIN-93M diet for maintenance thereafter (**Fig. 1B**). DATS was administered daily by gavage, and body weights were recorded weekly. Upon completion of the experiment, lung surface tumors were counted and photographed using an SMZ18 stereomicroscope (Nikon). A portion of the lung tissue was subjected to fixation in 4% paraformaldehyde, whereas the remaining samples were snap-frozen for storage at -80°C and future analysis.

2.3 Cell culture

MRC-5 cells from the Cell Collection Center of the Chinese Academy of Sciences and cultured in DMEM containing 10% fetal bovine serum and 0.1% gentamicin amphotericin-B. They were maintained at 37°C in a 5% CO_2 incubator, with the medium refreshed every two days.

2.4 Hematoxylin–eosin (HE) staining

For histological evaluation, following fixation in 4% paraformaldehyde, lung tissues were paraffin-embedded and cut into 4 μm sections. After dewaxing and rehydration, the sections were stained with hematoxylin and eosin (H&E) staining. The resulting histological sections were visualized and imaged using an Olympus light microscope.

2.5 Single-cell nuclear transcriptome sequencing of lung tissue

Mouse lung tissue samples that were rapidly frozen in liquid nitrogen were taken for single-nucleus RNA sequencing (snRNA-seq) analysis; Nuclear isolation and analysis were carried out by Novogene Biotechnology Co., LTD. The qualified cells were washed, nucleated and resuspended to prepare a single-cell nuclear suspension of an appropriate concentration. Single-cell RNA sequencing was carried out on all samples using the MobiCube® High Throughput Single Cell 3' RNA-Seq Kit (v2.1) at Novogene Co., Ltd. (Tianjin, China). Briefly, nuclei were encapsulated into droplets using a MobiNova-100 system and a microfluidic chip (MobiDrop Chip A Single Cell Kit v2.0), where mRNA was captured by oligo(dT)-coupled gel beads. Following reverse transcription, barcoded cDNA was amplified, and sequencing libraries were prepared with the High Throughput Single Cell 3' RNA-Seq Kit v2.0 and the 3' Single Index Kit. Sequencing of the final libraries was performed on an Illumina NovaSeq platform with a 150-bp paired-end configuration. Raw reads were quality-controlled with Fastp, and the gene-cell matrices generated by MobiVision v2.1 were imported into Seurat (v4.3.0) for downstream analysis, including dimensionality reduction, clustering, and snRNA sequence analysis.

2.6 Biochemical measurement

Oxidative stress and anti-oxidative stress related factors including malondialdehyde (MDA), catalase (CAT), superoxide dismutase (SOD), glutathione (GSH), and ROS were detected in serum, tissues, and cells using kits provided by Nanjing Jiancheng Bioengineering Co., Ltd.

2.7 Western blotting

Proteins were extracted from lung tissues with a whole cell lysis assay kit (KeyGEN, China). Following protein quantification (BCA kit, KeyGEN), aliquots (50 μg) were separated electrophoretically on 10% SDS-polyacrylamide gels and transferred to PVDF membranes. After blocking with 5% non-fat milk, the membranes were subjected to immunoblotting with specific primary antibodies (Nrf2, Keap1, HO-1, NQO1) at 4°C overnight, and then incubated with an HRP-linked secondary antibody for 2 h. Protein bands were imaged and quantified using ImageJ software.

2.8 Real-Time quantitative PCR (RT-qPCR)

Total RNA was isolated from mouse lung tissues and MRC-5 cells was carried out with the AxyPrep buffer system. Total RNA meeting quality thresholds was subjected to reverse transcription using the All-in-One First-Strand cDNA Synthesis SuperMix (TransGen Biotech) to generate cDNA. The resulting cDNA was amplified with Tip Green qPCR SuperMix (TransGen Biotech) in a real-time PCR system. Relative quantification of target genes was determined via the $2^{-\Delta\Delta Ct}$ algorithm following normalization to GAPDH or β-actin expression.

2.9 Immunoprecipitation assay（IP）

Protein lysates were prepared from lung tissues and MRC-5 cells using a Whole Cell Lysis kit (KeyGEN, China). Following centrifugation, protein concentrations were quantified using a BCA protein assay kit (KeyGEN, China). The proposed proteins were quantified into the same volume and the same protein content, and a portion was divided for subsequent WB experiments as Input control, and the remaining proteins were used for IP experiments. The IP proteins were added with antibodies at the amount of 1-2 μg of antibody to 1 mg, and subjected to gentle shaking at 4°C overnight. The appropriate amount of protein agarose beads underwent three washes with PBS, resuspended in an equal volume of PBS and combined with the immunoprecipitated protein complex, and shaken for 3 h at room temperature. The agarose beads with adsorbed antigen-antibody complexes received three successive washes with PBS and boiled for 10 min by adding 2X loading buffer. The same Western-blot fraction was subjected to SDS-PAGE gel electrophoresis.

2.10 CCK8 assay

Following a 24-hour adhesion period in 96-well plates, MRC-5 cells were exposed to NNK or DATS for 24 hours. Cell viability was then determined by adding 10 μL of CCK-8 reagent per well and incubating at 37°C for 4 hours before measuring the absorbance.

2.11 Immunofluorescence staining

Following deparaffinization, rehydration, and antigen retrieval, paraffin-embedded sections were blocked with 3% BSA (30 min, RT) and then incubated with primary antibody overnight at 4 °C. After washing, sections were incubated with a secondary antibody for 50 min at RT, stained with DAPI for nuclear visualization, and imaged by confocal microscopy.

2.12 Electrophoretic mobility shift assay (EMSA)

The binding activity of Nrf2 to the ARE was assessed using an EMSA kit (Beyotime, Nanjing, China). The same Western-blot fraction was extracted from mouse lung tissues for nuclear proteins (Inventbiotech, SC-003), the reaction system was configured according to the order of the EMSA instructions, and the labeled probes were combined with nuclear proteins in buffer (20-30 min, room temperature) to form the complexes, and nondenaturing polyacrylamide gel electrophoresis (low-temperature) was carried out to isolate the free probes from the protein-probe complexes.

2.13 Cellular heat transfer assay（CETSA）

The extracted MRC-5 cells from the control and DATS administration groups were homogeneously spiked into six PCR tubes of 100 μl each, followed by placing the PCR tubes containing 100 μl of cell suspensions in a gradient PCR instrument and heating them at a gradient temperature (50-60°C) for 4 min. Following the heating step, the samples were immediately frozen in liquid nitrogen and thawed at 37°C, with this freeze-thaw cycle repeated for three complete rounds. Subsequently, the supernatant was centrifuged and added to 6X loading buffer and boiled the samples for 10 min in preparation for Western blot analysis.

2.14 Drug affinity responsive target stability（DARTS）

The extracted MRC-5 cell proteins were quantified and separated into two equal parts, the dimethylsulfoxide (DMSO) group and DATS group, the DATS group was administered at a concentration of 0.94 μM, and the same volume of DMSO was given to the DMSO group, which was vortexed and mixed well and then incubated for 1 h at room temperature, and at the end of incubation, the proteins of each group were equally divided into four portions, and the appropriate amount of Pronase was added to dilute to the target concentration according to the protein content in each portion At the end of incubation, the proteins were divided into four portions and diluted to the target concentration by adding the appropriate amount of Pronase according to the protein content of each portion, vortexed and mixed, and then subjected to a 30-min incubation at room temperature.

2.15 Statistical analysis

Data are presented as mean ± standard deviation (SD). Statistical comparisons were performed by one-way ANOVA with appropriate post hoc tests using GraphPad Prism 8 software (San Diego, USA). A p-value of less than 0.05 was considered to indicate statistical significance.

3. Results

3.1 DATS suppresses NNK-promoted lung carcinogenesis in A/J mice

NNK administration induced a notable decline in body weight, which was effectively prevented by DATS treatment (**Fig. 1C**). To determine whether DATS confers protection against NNK-promoted lung cancer, lung and histological appearance analyses were performed after an 18-week intervention period across treatment groups, NNK exposure induced prominent tumor development in A/J mouse lungs, visible as white circular lesions (**Fig. 1D**). Quantification of tumor burden revealed that NNK stimulation significantly induced lung tumorigenesis ($P < 0.001$), with an average of 12.50 ± 4.50 tumors per mouse. DATS

intervention markedly suppressed both tumor initiation and progression, reducing the tumor count to 3.16 ± 1.84 per mouse (P < 0.01, **Fig. 1E**). Histopathological examination of HE-stained sections (**Fig. 1F**) corroborated these findings. Lung tissues from the NNK group exhibited variably differentiated tumors and extensive disruption of normal alveolar architecture, and the area of the necrotic tumor tissue has increased. Conversely, DATS-treated lungs showed substantially attenuated pathological differentiation and preserved alveolar structure, the area of the necrotic tumor region has significantly decreased. Collectively, our findings establish DATS as a strong chemopreventive agent against NNK-driven lung tumorigenesis in the A/J mouse model.

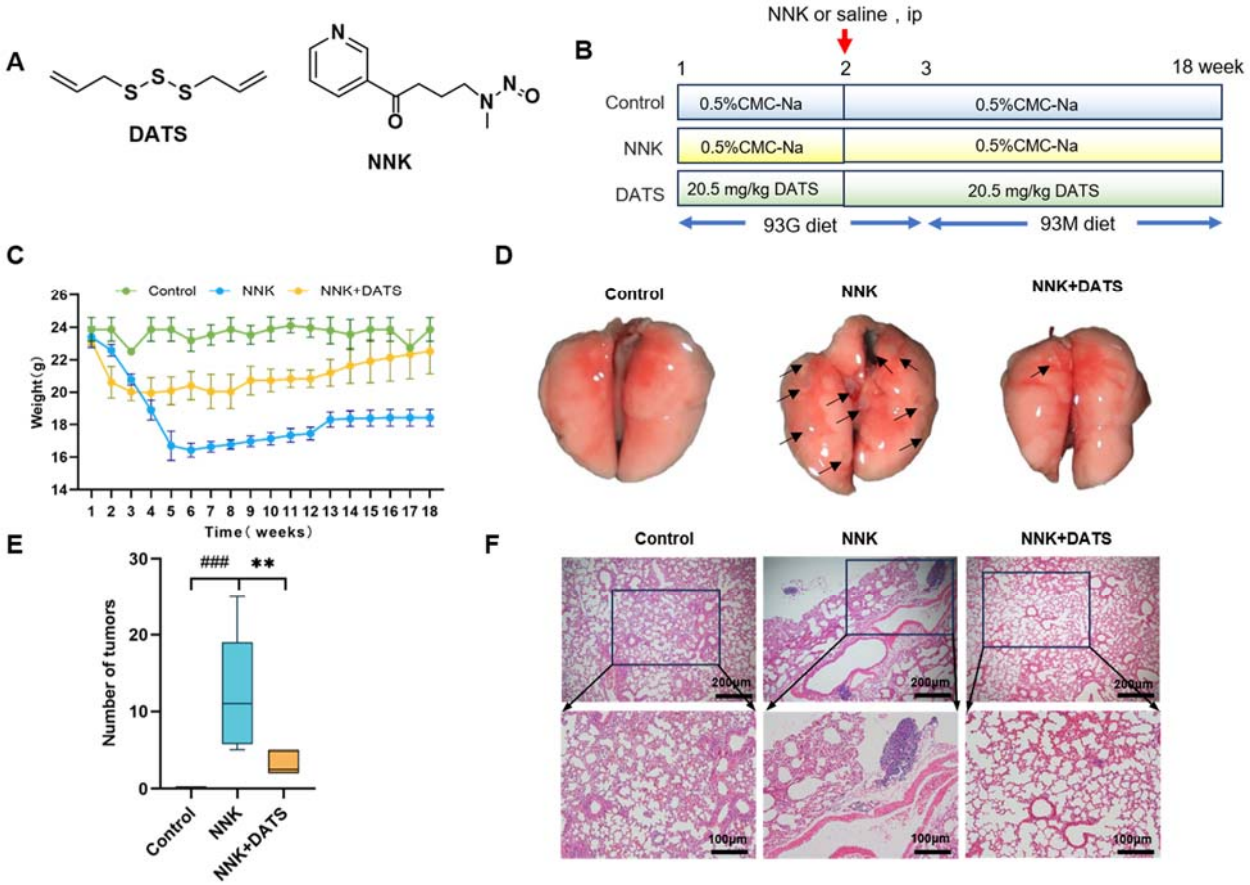

Fig. 1. DATS slows down the process of lung carcinogenesis in NNK-induced A/J mice. (A) Chemical structures of NNK and DATS. (B) Schematic overview of the experimental design. (C) Diagram of the change in body weight of mice during the experiment. (D) Representative images of the lungs. (E) The number of tumors was counted and analyzed at the endpoint of the experiment. (F) Representative images of HE staining of lung sections from each group. All photographs were obtained using a stereomicroscope. Using one-way ANOVA. Data are presented as mean ± SD (n=12). Compared with Control group, $^{###}P$ < 0.001, compared with NNK group, $^{**}P$ < 0.01.

3.2 DATS ameliorates NNK-induced lung oxidative stress injury in A/J mice

To assess the protective function of DATS against NNK- driven oxidative damage, we systematically measured key oxidative stress markers in murine serum and lung tissues. As shown in **Fig. 2A-D**, NNK exposure induced significant pulmonary oxidative injury relative to Controls, as substantiated by elevated MDA levels (P < 0.001) and CAT activity (P < 0.001) in lung tissue. DATS treatment effectively mitigated this damage, significantly reducing MDA accumulation (P < 0.001) and restoring CAT efficacy (P < 0.001). Systemically, NNK impaired antioxidant defenses through depleted serum GSH levels (P < 0.001) and

reduced SOD activity ($P < 0.001$), whereas DATS intervention significantly elevated GSH ($P < 0.001$) and enhanced SOD efficacy ($P < 0.001$). Collectively, DATS ameliorated NNK-induced oxidative stress markers, including lung MDA and CAT as well as serum SOD and GSH, confirming its potent antioxidant efficacy and providing a mechanistic foundation for further study.

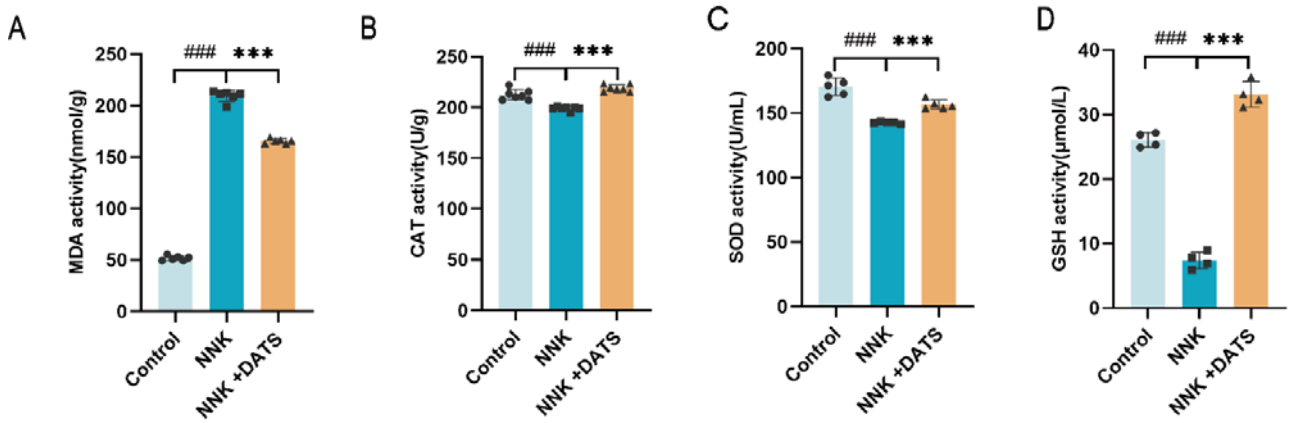

Fig. 2. DATS ameliorates NNK-induced lung oxidative stress injury in A/J mice (A) Determination of MDA level in mouse lung tissue (n=6). (B) Determination of CAT activity in mouse lung tissue (n=7). (C) Determination of serum SOD level in mice (n=5). (D) Determination of serum GSH level in mice (n=4). Using one-way ANOVA. Data are presented as mean ± SD. Compared with Control group, $^{\#\#\#}P < 0.001$, compared with NNK group, $^{***}P < 0.001$, $^{**}P < 0.01$.

3.3 Transcriptome sequencing elucidates the molecular mechanism underlying DATS inhibits NNK-induced lung carcinogenesis

We undertook snRNA-seq profiling of mouse lung tissues (Control, NNK, and DATS groups) to define the mechanism for DATS displays its chemopreventive effect on NNK-driven lung carcinogenesis (**Fig. 3A**). By unbiased clustering analysis, we successfully identified 19 initial cell clusters (**Fig. 3B**) and further precisely defined 17 cell types based on specific marker gene expression profiles (**Fig. 3C**). Analyses revealed that both NNK exposure and DATS treatment significantly altered the proportions of specific cell subpopulations, and these changes mainly involved alveolar type I epithelial cells (AT1), alveolar type II epithelial cells (AT2), B-cells, neuroendocrine cells (NE), and medullary dendritic cell subtype 2 (mDC2). DATS systematically protects and stabilizes the epithelial barrier involving AT2/AT1 cells by activating the Nrf2 pathway as a central driver, thereby maintaining AT2/AT1 cell homeostasis and preserving alveolar structural integrity. Concurrently, it enhances the immune surveillance capacity of mDC2/B cells and suppresses the abnormal activity of potentially pro-carcinogenic NE cells. The DATS-driven epithelial and immune cell populations synergize with the activation of the Nrf2 pathway, collectively establishing a multi-layered chemopreventive network (**Fig. 3D-E**). Cell type identification was performed using the following combinations of marker genes (**Fig. 3F**), AT1 cells were labeled with *Ager*, *Clib5*, and *Pdpn*; AT2 was labeled with *Sftpb*, *Sftpc*, *Sftpd*, *Etv5*, and *Sftpa1*, B cells were labeled with *Cd79a*, *Cd19*, *Ms4a1*, and *Ptprc*, NE cells were labeled with *Spint2*, and *Scgb3a2*, mDC2 cells were labeled with *Plin2*. This snRNA-seq analysis provides an important cellular molecular mapping basis for elucidating the chemopreventive mechanism of DATS. Expression profiling of *Nrf2* (NFE2L2) and its curated target genes identified significant alterations in *Nfe2l2*, *Akr1a1*, *Gstm1*, and *Gsta3* within the lung tissue (**Fig. 3G**). Overall, these

observations indicate that the Nrf2 signaling pathway contributes significantly to the inhibitory effects on lung cancer progression elicited by DATS.

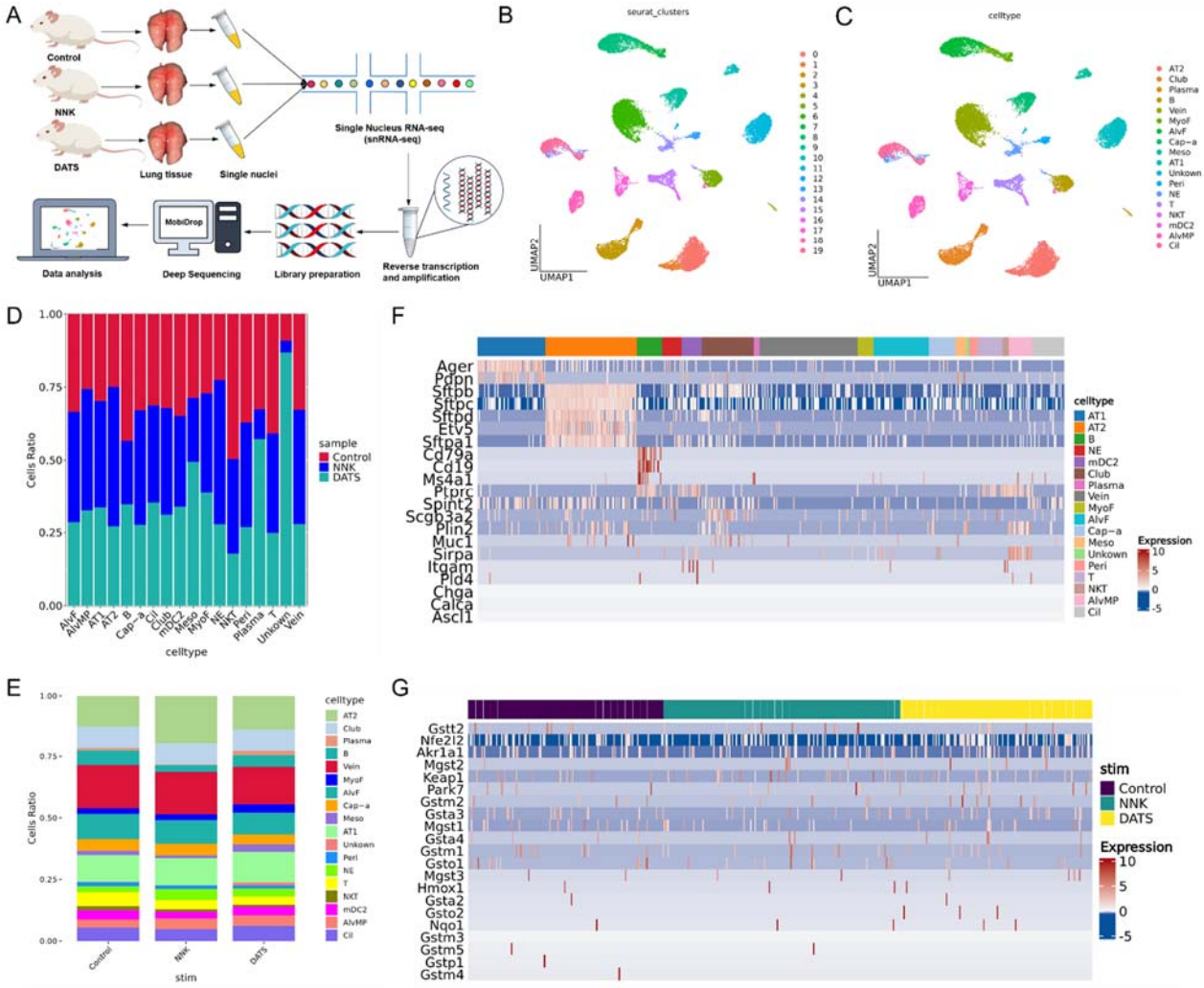

Fig. 3. sn-RNA sequencing reveals the molecular mechanism of DATS-mediated chemoprevention of lung cancer in NNK-exposed mice. (A) Schematic of the experimental and analytical workflow for single-nucleus RNA sequencing. (B) UMAP (Uniform Mobility Approximation and Projection) visualization of all captured nuclei. (C) UMAP of the integrated data identifying 17 cell lineages. (D-E) Proportional changes in major cell types across treatment groups. (F) Expression of canonical marker genes for each identified cell lineage. (G) Heatmap depicting expression of Nrf2-target genes in lung tissue.

3.4 DATS activates the Nrf2 pathway and enhances antioxidant responses

To further investigate the mechanism by which DATS attenuated NNK-induced oxidative stress injury, we analyzed the Nrf2 signaling pathway through integrated RT-qPCR, western blotting, immunofluorescence, and immunoprecipitation assay. RT-PCR revealed that DATS robustly induced the transcription of *Nrf2* ($P < 0.01$) and its key effector genes, *HO-1* ($P < 0.01$) and *NQO1* ($P < 0.001$), in the lung tissues of NNK-challenged mice (**Fig. 4A-C**). At the protein level, we found that DATS significantly increased the protein expression of Nrf2 ($P < 0.01$), HO-1 ($P < 0.01$), and NQO1 ($P < 0.01$) (**Fig. 4D-H**). Mechanistic studies revealed that in the cytoplasm, Nrf2 is sequestered by its repressor protein Keap1, forming an inactive complex under basal conditions. Whereas NNK stimulation induced Nrf2-Keap1 dissociation and nuclear translocation, DATS treatment further promoted this process (**Fig. 4I**). Complementary western blotting and immunofluorescence analyses confirmed enhanced nuclear Nrf2 protein expression in DATS-treated mice (*P*

< 0.01, **Fig. 4J-L**), collectively indicating that DATS indeed promoted the nuclear translocation of Nrf2. These data suggest that DATS activates Nrf2 and promotes antioxidant mechanism in NNK-driven mouse lung tissues.

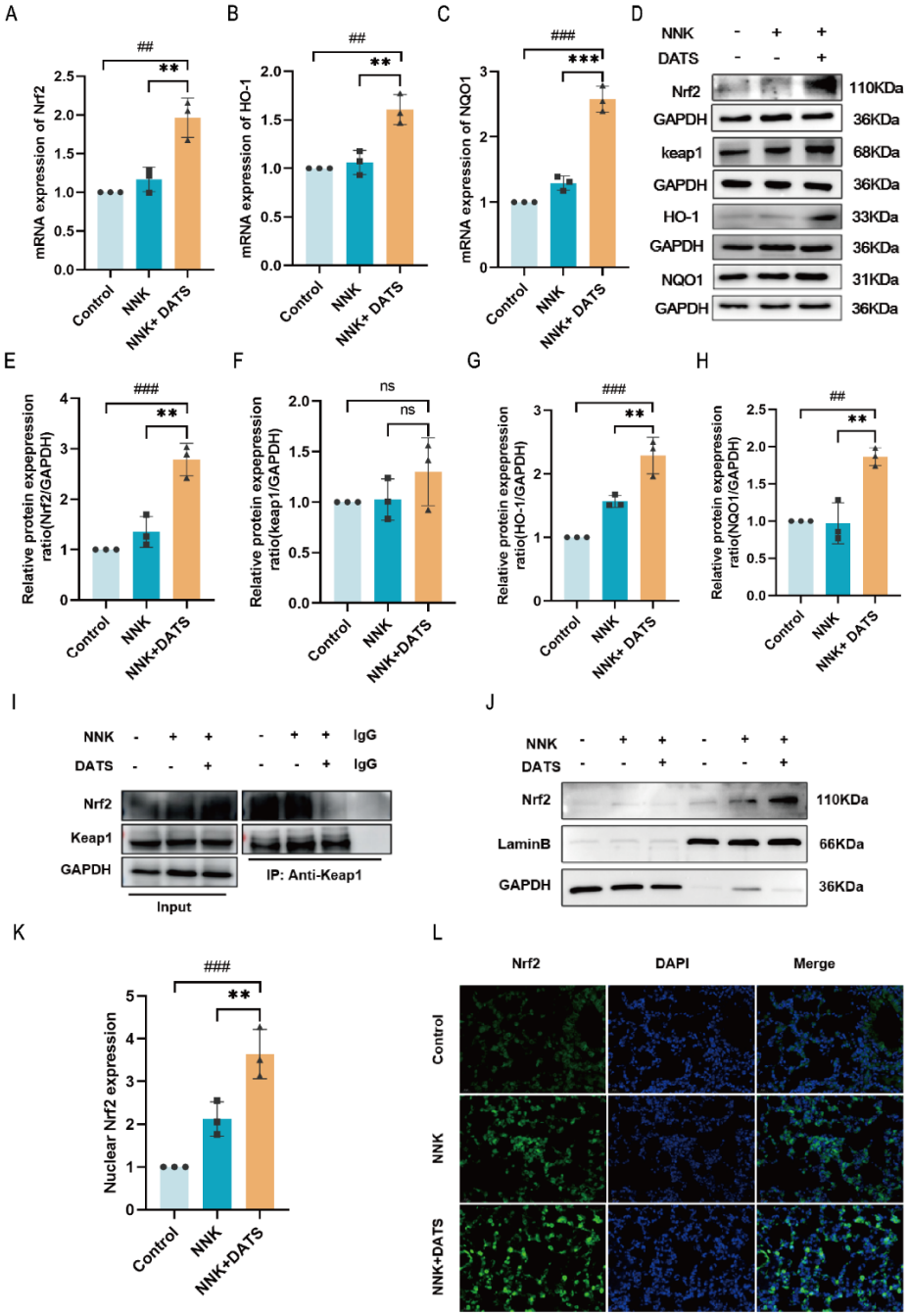

Fig. 4. DATS significantly activates the Nrf2 signaling pathway in A/J mice. (A-C) mRNA levels of *Nrf2*, *HO-1*, and *NQO1* in lung tissues of A/J mice. (D) Western blotting of Nrf2 pathway-related proteins in lung tissues of A/J mice. (E-H) Protein levels of Nrf2, HO-1, NQO1 in lung tissues of A/J mice. (I) Immunoprecipitation assay for Keap1-Nrf2 protein interaction. (J) Nrf2 protein blotting in cytoplasm and nucleus in lung tissues of A/J mice. (K) Nrf2 protein levels in nuclei in lung tissues of A/J mice. (L) Representative images of Nrf2 immunofluorescence staining in lung tissues of A/J mice. Using one-way ANOVA. Data are presented as mean ± SD (n = 3). Compared with Control group, $^{###}P < 0.001$, $^{##}P < 0.01$, compared with NNK group, $^{***}P < 0.001$, $^{**}P < 0.01$.

3.5 DATS confers cytoprotection against NNK-induced oxidative damage in MRC-5 Cells

Building on this, we examined DATS on NNK-injured MRC-5 cells at the cellular level. Firstly, we established its safety profile in MRC-5 cells using CCK-8 assays. MRC-5 cells were pretreated with following

a 24-hour exposure to varying concentrations of DATS. Results displayed MRC-5 cell viability was not affected by treatment with DATS at concentrations up to and including 7.5 μM (**Fig. 5A**). After establishing a non-cytotoxic dose, DATS demonstrated a protective effect against NNK-driven injury in MRC-5 cells. **Fig. 5B** shows that while NNK markedly decreased cell viability compared to controls, co-treatment with DATS significantly attenuated this loss and maintained high cell viability. We further quantified oxidative stress markers in NNK-exposed cells. Fluorescence imaging and enzymatic analysis confirmed NNK triggered substantial ROS accumulation, which DATS treatment markedly suppressed (**Fig. 5C-D**). Concurrently, DATS restored the decreased levels of GSH, CAT and SOD caused by NNK exposure, and also reduced the level of MDA (**Fig. 5E-H**). Collectively, these results demonstrate DATS protects MRC-5 cells from NNK-driven cytotoxicity by mitigating oxidative damage.

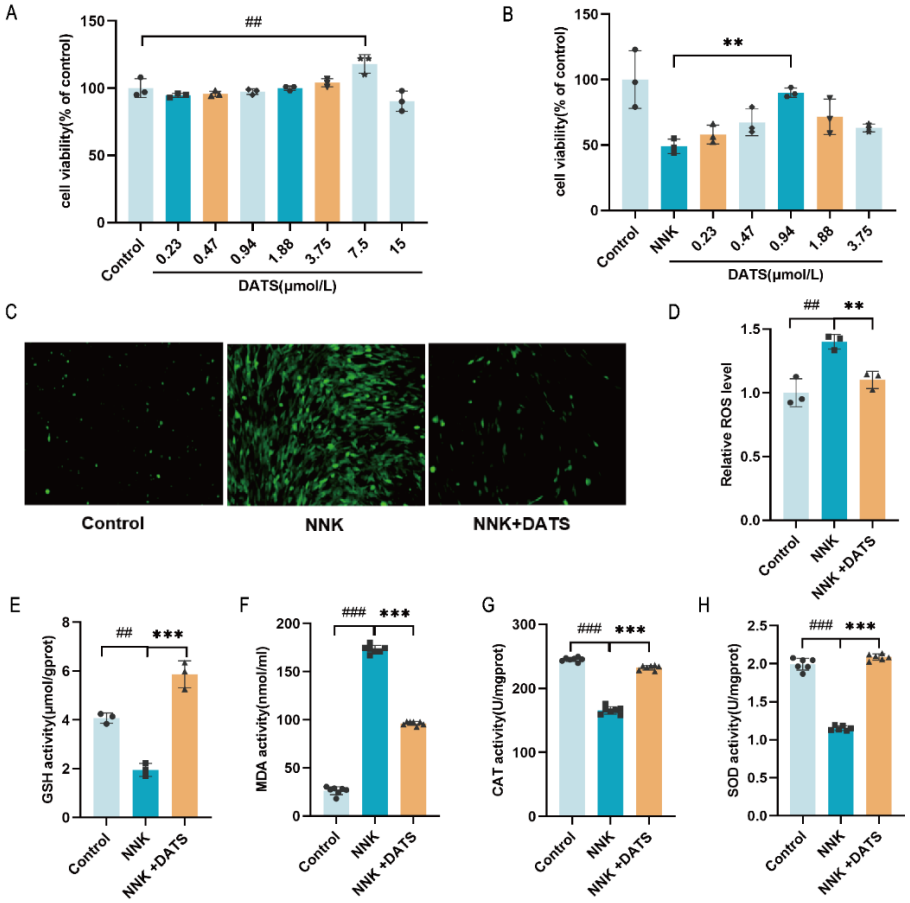

Fig. 5. DATS attenuates NNK-induced cellular oxidative damage in MRC-5 cells. (A) MRC-5 cells were treated with DATS (0, 0.23, 0.47, 0.94, 1.88, 3.75, 7.5, and 15 μM) alone for 24 h. Cell viability was detected by CCK8 assay (n=3). (B) MRC-5 cells were co-incubated with NNK (0.6 mg/mL) and DATS (0.23, 0.47, 0.94, 1.88, 3.75 M) for 24 h. Cell viability was detected by CCK8 assay (n=3). (C) The level of intracellular ROS was detected by fluorescence microscopy. (D) Intracellular ROS fluorescence values were detected using a multifunctional enzyme marker (n=3). (E) GSH content was detected by GSH activity kit (n=3). (F) Cellular MDA level was detected (n=7). (G) Cellular CAT level was detected (n=7). (H) Cellular SOD level was detected (n=6). Using one-way ANOVA. Data are presented as mean ± SD. Compared with Control group, $^{###}P < 0.001$, $^{##}P < 0.01$, compared with DATS group, $^{***}P < 0.001$, $^{**}P < 0.01$.

3.6 DATS induces Nrf2 pathway activation, leading to the subsequent upregulation of antioxidant genes in MRC-5 cells

Following the confirmation that DATS mitigates NNK-induced oxidative injury, we delineated its mechanism through molecular analyses. RT-qPCR demonstrated DATS significantly upregulated mRNA

levels of *Nrf2* ($P < 0.01$), *HO-1* ($P < 0.01$) and *NQO1* ($P < 0.05$) in NNK-treated MRC-5 cells (**Fig. 6A-C**). Western blot analysis corroborated these findings, revealing increased Nrf2, HO-1, and NQO1 protein expression in DATS-treated cells versus NNK, while Keap1 levels remained unchanged (**Fig. 6D-H**). Co-IP confirmed DATS promoted dissociation of the Keap1-Nrf2 complex (**Fig. 6I**). Concomitantly, DATS facilitated Nrf2 nuclear translocation, as evidenced by elevated nuclear Nrf2 protein in western blotting (**Fig. 6J-K**) and immunofluorescence (**Fig. 6L**). EMSA further revealed enhanced Nrf2 binding to AREs following DATS treatment (**Fig. 6M**). Taken together, our results demonstrate that DATS activates the Nrf2-ARE signaling pathway by inducing Keap1-Nrf2 dissociation, enhancing Nrf2 expression, and promoting its nuclear translocation, leading to the transactivation of antioxidant genes.

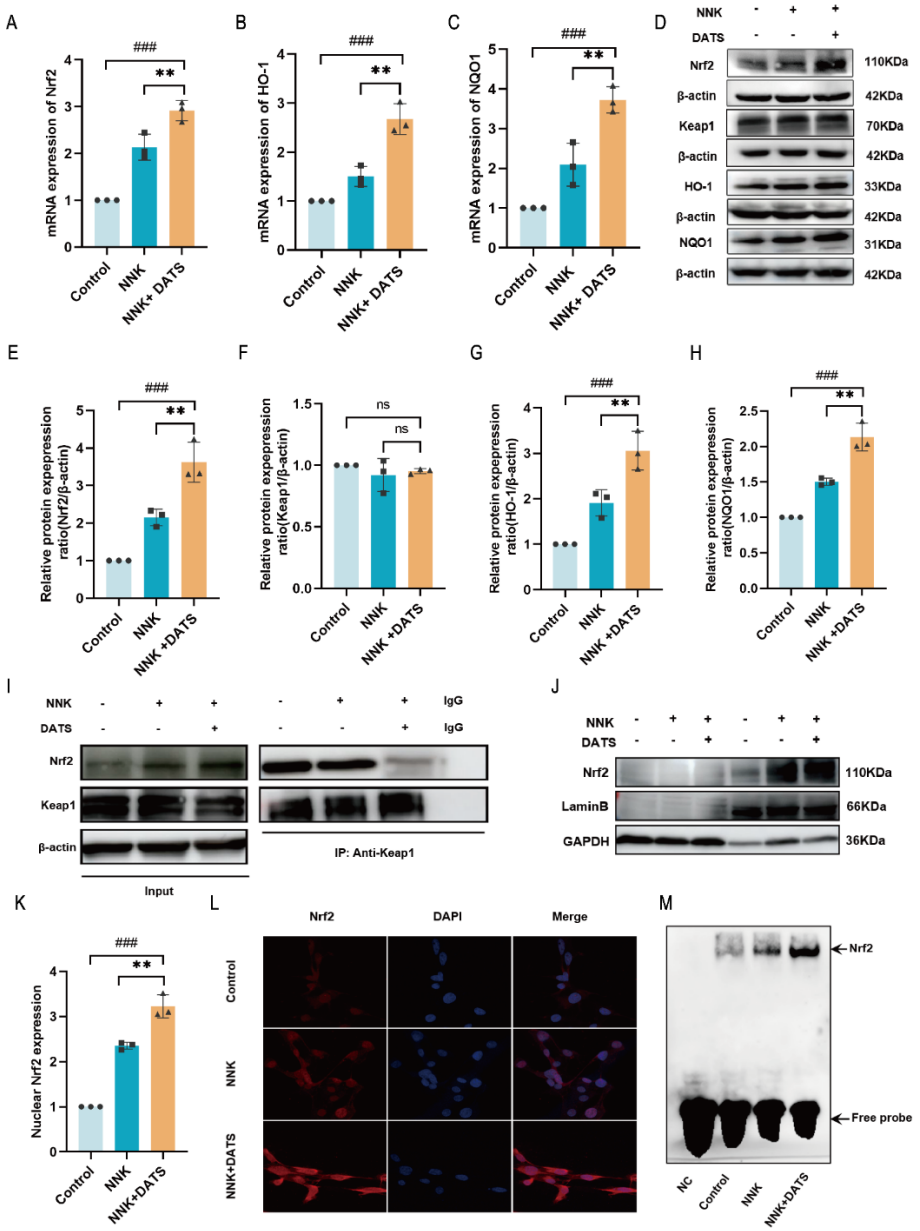

Fig. 6. DATS activates Nrf2 signaling and facilitates the antioxidative pathway in MRC-5 cells. (A-C) mRNA levels of *Nrf2*, *HO-1*, and *NQO1* in MRC-5 cells. (D) Protein blotting diagram of Nrf2 pathway-related proteins in MRC-5 cells. (E-H) Protein levels of Nrf2, HO-1, NQO1 in MRC-5 cells. (I) Immunoprecipitation assay for Keap1-Nrf2 protein interaction. (J) Nrf2 protein blotting maps in the cytoplasm and nucleus in MRC-5 cells. (K) Nrf2 protein levels in the nucleus in MRC-5 cells. (L) Representative graph of Nrf2 immunofluorescence staining in MRC-5 cells. (M) The binding affinity between Nrf2-ARE was evaluated using EMSA. Using one-way ANOVA. Data are presented as mean ± SD (n=3). Compared with Control group, $^{\#\#\#}P < 0.001$, compared with NNK group, $^{**}P < 0.01$.

3.7 DATS directly binds Keap1 to activate Nrf2-dependent antioxidant mechanisms

To elucidate whether DATS directly interacts with the Keap1 protein and facilitates the dissociation of Nrf2, CETSA, DARTS, and molecular docking were employed for validation. CETSA revealed Keap1 in untreated MRC-5 cells degraded initiation at 54°C with complete degradation at 56°C. Conversely, in the DATS-treated group, the expression of the Keap1 protein remained at a relatively high level even at 56°C (**Fig. 7A-B**), indicating that DATS significantly enhances the thermal stability of the Keap1 protein. DARTS corroborated this stabilization, showing reduced Keap1 proteolysis at 1% pronase in DATS-treated groups versus controls (**Fig. 7C**). Molecular docking elucidated the structural mechanism. DATS competes with Nrf2 for binding to the Keap1 Kelch domain, forming a stable complex. Within the Kelch domain pocket, the allyl group of DATS forms a hydrophobic cage effect with hydrophobic residues Val463, Val604, Ile416, and Leu365. Additionally, its sulfur atom forms a polar contact with Arg415 and engages in multiple backbone interactions with the Gly509-Gly558 flexible region, such as Gly462, Gly464, Gly559, and Gly603 (**Fig. 7D-E**). This binding directly occupies the ETGE motif binding cavity of Nrf2, competitively inhibiting the Nrf2-Keap1 binding through steric hindrance and local conformational stabilization. To more directly prove that Keap1 is the target of DATS, siRNA was transfected into MRC-5 cells to knock down the expression of Keap1, and the effect of DATS on the cells was observed to determine if there was still a significant difference compared with the NNK group. After screening the optimal transfection conditions, the CCK8 method was used to detect the protective effect of DATS on NNK-induced cells after Keap1 knockdown. The results showed that under the background of Keap1 knockdown, there was no significant difference in cell viability between the DATS and NNK groups (**Fig. 7G**). Western Blot was used to detect the protein expression of Nrf2 and Keap1 after Keap1 knockdown. The results showed that after Keap1 was knocked down, the protein expression of Nrf2 in the DATS group did not significantly increase compared with the NNK group (**Fig. 7H-I**). Therefore, under the background of Keap1 knockdown, the binding effect of DATS with Keap1 was inhibited, and thus the activation effect on Nrf2 also disappeared. The aforementioned findings consistently demonstrate that DATS directly interacts with the Keap1 protein, competitively occupying the Kelch domain to enhance the structural stability of Keap1 and facilitate the dissociation of Nrf2, thereby confirming Keap1 as the direct molecular target of DATS.

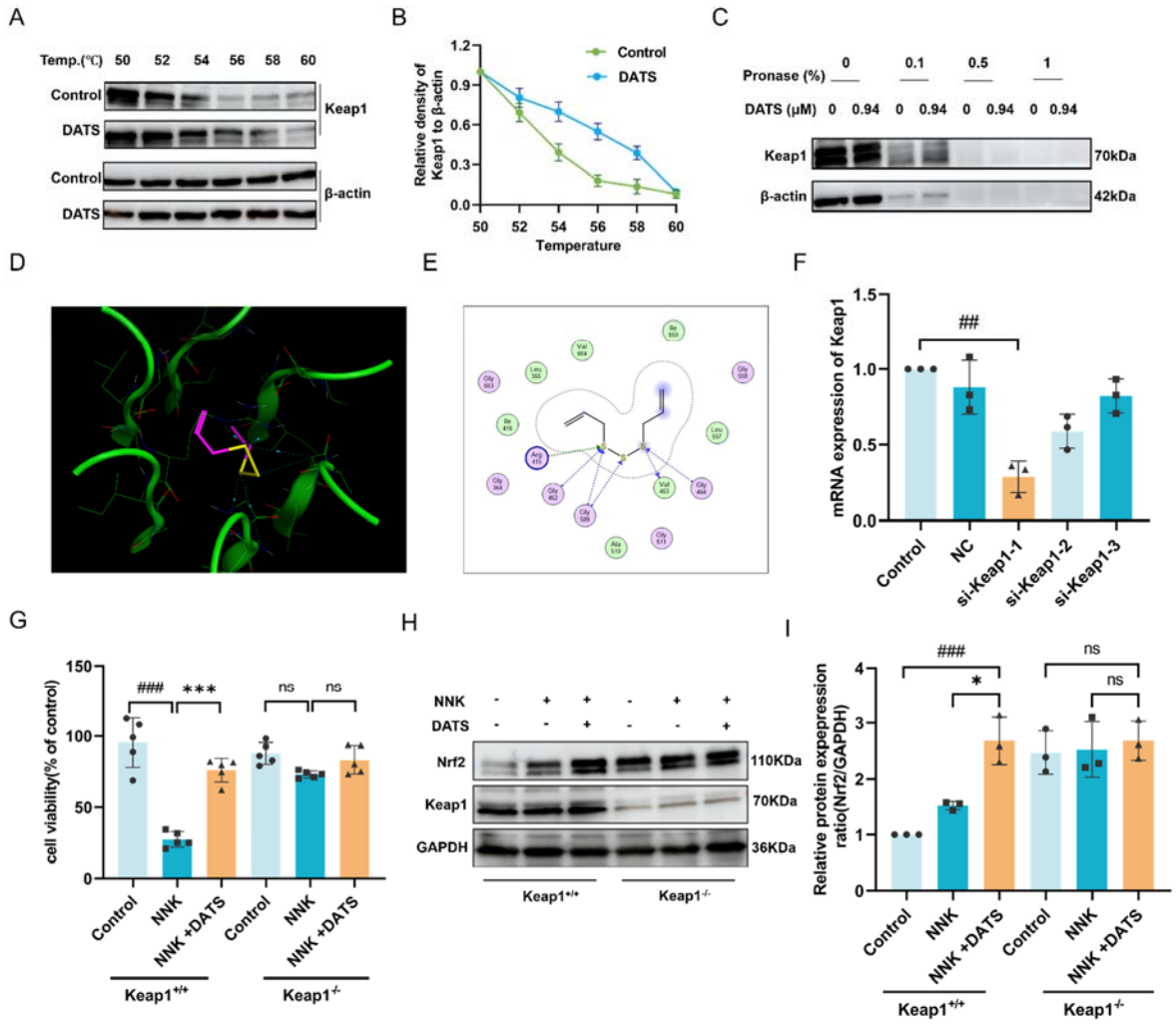

Fig. 7. DATS binds directly to Keap1, stabilizes its structure, and promotes Nrf2 dissociation. (A-B) CETSA showed DATS enhanced Keap1 thermal stability in MRC-5 cells, maintaining high protein levels at 56 °C (n=3). (C) DARTS confirmed DATS reduced pronase-dependent Keap1 degradation (n=3). (D-E) Molecular docking indicated DATS binds the Keap1 Kelch domain via hydrophobic and polar interactions, competitively blocking Nrf2 binding. (F) Screening of transfection conditions for Keap1 knockdown by siRNA. (G) CCK8 assay to detect the protective effect of DATS on MRC-5 cells after Keap1 knockdown by siRNA. (H-I) Protein levels of Nrf2 and Keap1 in MRC-5 cells after Keap1 knockdown by siRNA. Using one-way ANOVA. Data are presented as mean ± SD (n=3). Compared with Control group, $^{###}P < 0.001$, $^{##}P < 0.01$, compared with NNK group, $^{***}P < 0.001$, $^{**}P < 0.01$, $^{*}P < 0.05$.

3.8 Abrogation of Nrf2 activity reverses DATS-mediated protection against NNK-induced cytotoxicity in MRC-5 cells

To investigate whether Nrf2 mediates the protective effects of DATS, we employed the specific Nrf2 inhibitor ML385. Prior to pathway inhibition studies, a CCK-8 assay verified that ML385 failed to produce adverse effect on MRC-5 cell viability (**Fig. 8A**). DATS effectively mitigated the NNK-induced pro-oxidant/antioxidant imbalance in MRC-5 cells by normalizing ROS, MDA, GSH, CAT, and SOD levels. The co-application of ML385 with DATS notably blunted this corrective action (**Fig. 8B-G**). Western blot analysis confirmed that DATS upregulated the protein expression of Nrf2 and its downstream targets, HO-1 and NQO1, in mouse lung tissues. However, this induction was markedly suppressed by ML385 co-treatment (**Fig. 8H-L**). Collectively, these findings identify Nrf2 activation as the essential mechanism through which

DATS exerts its protective effect against NNK-induced lung injury, positioning Nrf2 as the central mediator of DATS-driven chemoprevention.

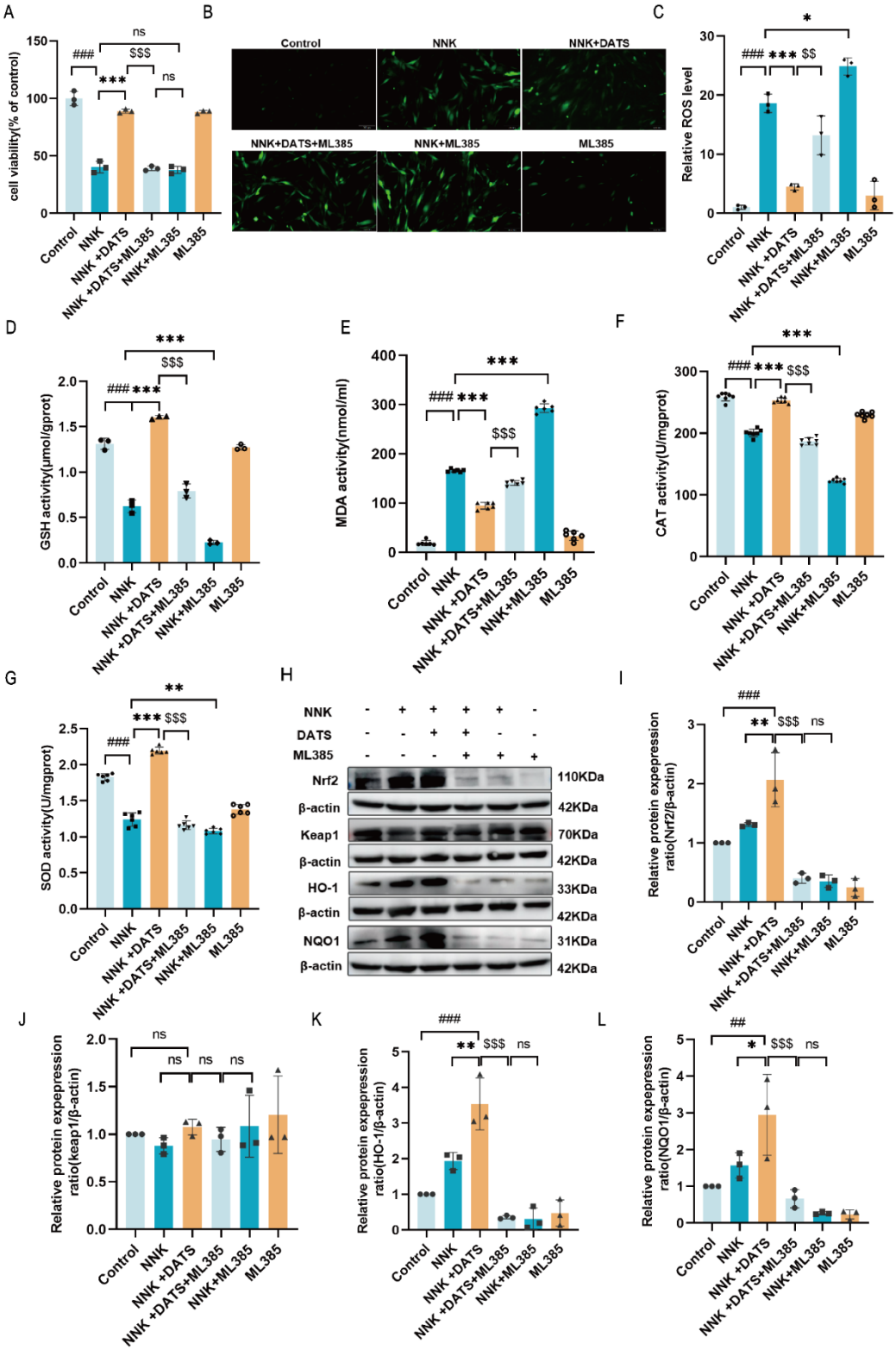

Fig. 8. Pharmacological inhibition of Nrf2 abrogates the protective effect of DATS against NNK-induced injury in MRC-5 cells. (A) CCK-8 assay was performed to evaluate the cytotoxicity of ML385. (B) Representative fluorescence images showing ROS levels in MRC-5 cells. (C) Quantitative analysis of ROS levels in MRC-5 cells. (D-G) Determination of GSH, MDA, CAT, and SOD levels in MRC-5 cells, respectively. (H) Representative Western blot images of proteins in MRC-5 cells. (I-L) Quantitative analysis of Nrf2, Keap1, HO-1, and NQO1 protein levels in MRC-5 cells, respectively. Using one-way ANOVA. Data are presented as mean ± SD (n=3). Compared with Control group, $^{###}P < 0.001$, $^{##}P < 0.01$, compared with NNK group, $^{***}P < 0.001$, $^{**}P < 0.01$, $^{*}P < 0.05$, compared with NNK+DATS+ML385 group, $^{\$\$\$}P < 0.001$.

4. Discussion

Lung cancer ranks among the most common cancers worldwide, with approximately 2.2 million new cases and 1.8 million deaths annually. Dietary patterns are key determinants of human health, and dietary fiber intake has been shown to reduce the risk of lung cancer [36]. Garlic, a versatile ingredient combining culinary flavor and medicinal properties, serves as a vital spice in global culinary traditions. Its rich bioactive compounds and pharmacological effects have long been utilized in the prevention and adjunctive treatment of various human diseases. Epidemiological evidence indicates that increasing dietary intake of allium vegetables (such as garlic) may help reduce the risk of developing multiple diseases, including lung cancer. A population-based case-control study further revealed a significant inverse association between consuming raw garlic at least twice weekly and the risk of lung cancer [37]. It has been demonstrated that garlic exerts its anti-lung cancer effects through its organosulfur compounds, and DATS is one of the most bioactive components among these compounds, exhibiting potential to prevent lung cancer progression [38].

Our findings comprehensively explored the chemopreventive efficacy of DATS and its underlying mechanisms using both an NNK-driven lung adenocarcinoma model in A/J mice and an MRC-5 cell injury model. Our results provide evidence that DATS significantly suppressed NNK-driven lung tumorigenesis and reduced tumor burden. *In vitro* studies further confirmed that DATS treatment effectively alleviated NNK-driven oxidative injury in MRC-5 cells, as evidenced by a significant improvement in oxidative stress markers and an obvious enhancement in antioxidant enzyme activities. Mechanistic studies showed that DATS activated the Nrf2-mediated antioxidant defense system by targeting and regulating the Keap1-Nrf2 signaling pathway. Collectively, our data provide strong support for the use of DATS in preventing smoking-induced lung cancer, thereby paving the way for chemoprevention as a practical approach to mitigate lung cancer burden [39-43].

Our findings indicate that at a dose of 23 mg/kg, DATS exhibits significant chemoprotective effects against NNK-induced lung cancer in the established A/J mouse model. The DATS dosage used in this study was determined based on our previous research. We previously demonstrated that administering 50 mg/kg garlic oil to A/J mice provided chemoprotective effects against NNK-induced lung cancer. Since garlic oil contains 46.35% ± 0.32% DATS, the DATS dosage in this study was converted to 23 mg/kg [31]. This model is particularly relevant for such studies due to its defined genetic susceptibility, high incidence of both spontaneous and chemically-induced lung tumors, and pathological features closely mirroring human lung cancer [44-46]. Consistent with the known carcinogenic effects of NNK [11], mice treated with NNK exhibited reduced body weight and developed numerous visible lung tumors, accompanied by severe histopathological alterations, including disrupted alveolar architecture and varying degrees of cellular differentiation as evidenced by HE staining. Importantly, DATS intervention effectively prevented NNK-induced weight loss and markedly suppressed tumor burden, preserving near-normal lung histoarchitecture. These results show that DATS suppresses the progression of NNK-driven lung tumors in this model. The protective mechanism of DATS appears to be strongly linked to its ability to counteract

NNK-induced oxidative stress, a well-documented consequence of this carcinogen [47-49], and to systematically assess the antioxidative effect of DATS, we quantified the pulmonary and serum of NNK-exposed mice oxidative stress burden. The present study revealed that NNK exposure significantly increased MDA levels, a key marker of lipid peroxidation, which was accompanied by a substantial decrease in CAT activity. These alterations collectively pointed to severe oxidative injury in the local tissue. DATS treatment effectively mitigated this damage, significantly lowering MDA content and restoring CAT activity towards control levels. Systemically, NNK treatment led to a significant impairment of the antioxidant defense system, as reflected by markedly decreased serum SOD activity and GSH levels. DATS administration significantly ameliorated this systemic oxidative stress, enhancing both serum SOD activity and GSH levels. These results, concordant with the findings of Yang et al [50], collectively demonstrate that DATS enhances both lung tissue and systemic antioxidant capacity. The restoration of key antioxidant enzymes, like as CAT and SOD, and the crucial antioxidant molecule GSH, alongside the reduction in MDA, strongly supports the conclusion that DATS confers protection against NNK-induced lung carcinogenesis, at least in part, by bolstering the host's antioxidant defenses and attenuating oxidative damage.

Chronic oxidative stress is a key pathological mechanism in lung cancer. To this end, we examined the antioxidant mechanism of DATS in NNK-driven lung cancer using A/J mice [51]. Nrf2 and its interacting partner Keap1 are pivotal in preserving redox homeostasis. In mammalian cells, Nrf2 governs the expression of numerous genes. Given its pivotal role in maintaining cellular redox homeostasis, Nrf2 has become a leading therapeutic target for numerous oxidative stress-related disorders [52, 53]. To elucidate the mechanism by which DATS mitigates NNK-induced oxidative damage, we examined the Nrf2 pathway. DATS treatment was found to activate the Nrf2 pathway, as evidenced by elevated level of Nrf2, HO-1, and NQO1 at both transcriptional and translational levels in mouse lung tissues. This activation follows the canonical mechanism: upon disruption of the Keap1-Nrf2 complex by stress signals, Nrf2 moves to the nucleus, dimerizes with small Maf proteins, and combineds with AREs to drive the expression of antioxidant genes [52, 54, 55]. Co-IP analysis revealed that both NNK and DATS facilitated the separation of Nrf2 from Keap1 and facilitate the nuclear translocation of Nrf2, with DATS exhibiting a more pronounced effect. This enhanced nuclear accumulation of Nrf2 in the DATS-treated group was consistently confirmed by Western blot and immunofluorescence. The Nrf2-ARE pathway regulates a broad array of cytoprotective genes, including those encoding antioxidant-related genes and phase II detoxification enzymes. While constitutive Nrf2 activation has been implicated in conferring a survival advantage to tumor cells against oxidative stress, chemotherapy, and radiotherapy, thereby exhibiting potential pro-tumorigenic effects [15, 56-58], its controlled activation remains a valuable therapeutic strategy for chemoprevention by bolstering antioxidant defenses. These findings support the conclusion that DATS alleviates NNK-induced oxidative stress in mouse lung tissue by activating the Nrf2 pathway, which promotes Keap1-Nrf2 dissociation, facilitates Nrf2 nuclear translocation, and subsequently upregulates key antioxidant and detoxifying enzymes to enhance cellular defense.

To further validate our in vivo findings and clarify the molecular mechanism of DATS via the Nrf2 pathway, we turned to an in vitro system. To this end, a cellular model of NNK-induced damage was generated in MRC-5 cells. MRC-5 cells, due to their genetic stability derived from normal lung tissue, comparability with cancer cells, and specific responses to drugs/stress, have become an indispensable model in lung cancer research [59]. Mirroring our in vivo observations, DATS treatment in MRC-5 cells attenuated oxidative stress and upregulated the transcript and protein levels of Nrf2 and its downstream targets, HO-1 and NQO1. Notably, Co-IP assays similarly confirmed the dissociation of the Keap1-Nrf2 complex. Crucially, the results of EMSA demonstrated that DATS significantly enhanced Nrf2 binding activity to ARE, revealing a core mechanism of DATS-mediated lung protection through direct Nrf2 pathway regulation.

To identify the specific molecular targets through which DATS activates the Nrf2 pathway, we employed a multi-dimensional technical strategy for validation. We first interrogated potential DATS-Keap1 binding using CETSA to assess ligand-induced shifts in Keap1's thermal stability. Data from this study indicate that DATS treatment significantly increased the thermal denaturation temperature of Keap1, indicating that it enhances the conformational stability of Keap1 by binding to it. This phenomenon is consistent with the CETSA characteristics of Keap1-targeted inhibitors and aligns with the classic principle of drug-target complex resistance to thermal dissociation [60, 61]. Given that CETSA only reflects intracellular binding, we further used DARTS to exclude cellular environmental interference. After trypsin treatment, the degradation rate of Keap1 protein in the DATS-bound group decreased, confirming that its direct binding protects Keap1 from proteolytic hydrolysis. Molecular docking results showed that the allyl sulfide structure of DATS can embed into the Kelch domain of Keap1, forming stable hydrogen bond interactions with key amino acid residues such as Arg415. To provide a more direct proof that Keap1 is the target of DATS, we transfected siRNA to knockdown Keap1 in MRC-5 cells. Under the knocked-down condition, there were no significant differences in cell viability changes and Nrf2 protein expression between the DATS and NNK groups. Therefore, after Keap1 was knocked down, the binding effect of DATS with Keap1 was inhibited, and as a result, the activation effect on Nrf2 also disappeared. These results collectively demonstrate that Keap1 is the direct target of DATS for activating the Nrf2 pathway.

Given that Nrf2 nuclear translocation was increased and ARE reporter gene activity was elevated in the DATS-treated group of MRC-5 cells, and that these alterations were significantly linked to the mitigation of redox imbalance in which Nrf2 was involved, we further validated the necessity of the Nrf2 pathway by pharmacological inhibition assays. Pretreatment of MRC-5 cells with the specific Nrf2 inhibitor ML385 [62] effectively blocked DATS-induced Nrf2 transcriptional activity. ML385 completely abolished the DATS-mediated upregulation of Nrf2, HO-1, and NQO1 protein expression and significantly reversed the antioxidant protective effects of DATS, confirmed that the activation of the Nrf2 pathway is crucial for the protective effect of DATS on cells.

Except for the core Nrf2 antioxidant pathway, DATS may exert chemopreventive effects against lung cancer through multi-target synergistic mechanisms. Our prior work demonstrated that in NNK-exposed

MRC-5 cells, DATS significantly reduced levels of the pro-inflammatory mediators TNF-α and IL-6 and inhibited phosphorylation of the NF-κB p65 subunit, indicating that DATS also possesses anti-inflammatory activity [63]. Furthermore, studies suggest DATS can inhibit carcinogenesis in other models, such as preventing BaP-induced breast epithelial cell transformation by suppressing aryl hydrocarbon receptor (AhR) activity and enhancing DNA repair capacity [64]. This implies that DATS-mediated Nrf2 activation may influence a broader regulatory network beyond canonical antioxidant genes, potentially modulating inflammation and genotoxic stress responses. Although mapping these intricate networks was beyond our current scope, the identified multi-target synergy presents a compelling framework for understanding the broad efficacy of DATS, particularly against the complex carcinogenic milieu of tobacco smoke.

While our study confirms the chemopreventive role of DATS in NNK-driven lung tumor via the Keap1-Nrf2 axis, several limitations should be noted. First, although Nrf2 activation is established as a key mechanism, the direct interaction pattern of DATS with Keap1 is premised on, yet not fully delineated. This is a significant question, as Keap1 contains multiple critical cysteine residues documented as binding targets for numerous Nrf2 activators [65]. To unequivocally determine the binding modality of DATS, future studies should employ structural biology techniques, such as X-ray crystallography or cryo-EM, to resolve the DATS-Keap1 complex structure. Secondly, in terms of translational medicine, this study showed significant effects with 23 mg/kg of DATS in a mouse model, but its bioavailability in humans has not yet been evaluated. It is worth noting that allicin-like compounds generally have low oral bioavailability [66, 67]. Therefore, developing more stable DATS derivatives or novel delivery systems may be an important direction for improving its clinical translational value. Thirdly, regarding long-term safety issues, although Nrf2 activation exhibits protective effects in the short term, long-term excessive activation of Nrf2 may promote the development of certain cancers [68, 69]. This study only observed the effects of short-term intervention and lacked an assessment of the safety of long-term use of DATS. Future studies should conduct longer-term animal experiments to monitor the potential risks associated with the prolonged induction of Nrf2 pathway activity.

5. Conclusion

Our findings establishes that DATS provides significant chemoprevention against NNK-driven lung tumorigenesis in vivo and alleviates oxidative damage in MRC-5 cells in vitro. Mechanistically, DATS modulates Keap1-Nrf2 axis, activating the Nrf2 antioxidant pathway, thereby mitigating oxidative stress accumulation and restoring redox homeostasis (**Fig. 9**). These findings, consistently validated through complementary *in vivo* and *in vitro* experiments, underscore the capacity of DATS as a natural product for lung tumor chemoprevention. In view of its well-defined molecular target of Keap1-Nrf2 axis and potent bioactivity, DATS is expected to become a promising candidate drug, particularly for preventing tobacco carcinogen-associated lung tumor.

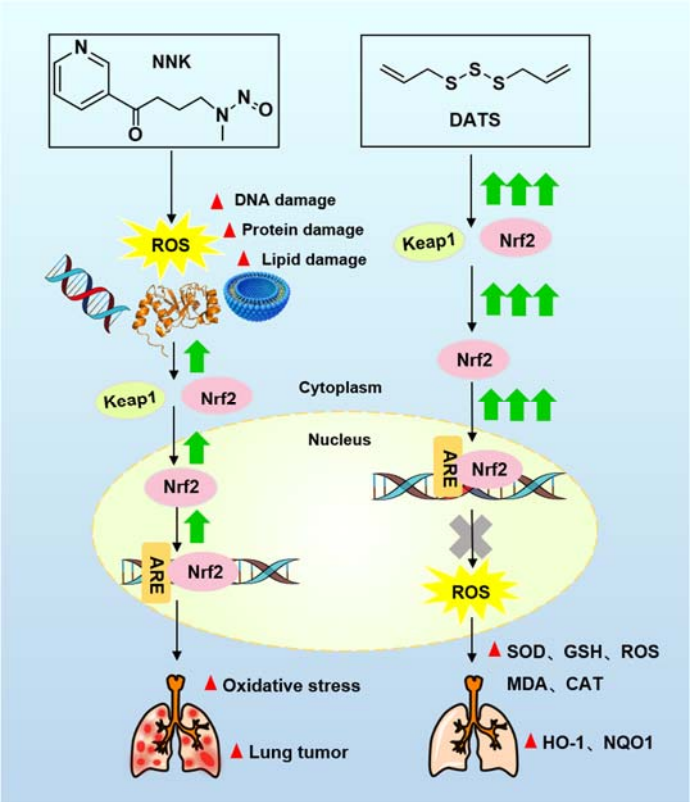

Fig. 9. Schematic diagram of DATS regulating the Keap1-Nrf2 axis, activating the Nrf2 pathway, reducing the accumulation of oxidative stress and restoring the redox balance mechanism.

Declaration of competing interest

The authors declare no competing financial interests or personal relationships that might bias this research.

Data availability

Data will be made available on request.

References

1. Sung, H., Ferlay, J., Siegel, R.L., et al. (2021). Global Cancer Statistics 2020: GLOBOCAN Estimates of Incidence and Mortality Worldwide for 36 Cancers in 185 Countries. CA Cancer J Clin *71*, 209-249. 10.3322/caac.21660.
2. Cao, W., Chen, H.D., Yu, Y.W., et al. (2021). Changing profiles of cancer burden worldwide and in China: a secondary analysis of the global cancer statistics 2020. Chin Med J (Engl) *134*, 783-791. 10.1097/cm9.0000000000001474.
3. Han, B., Zheng, R., Zeng, H., et al. (2024). Cancer incidence and mortality in China, 2022. J Natl Cancer Cent *4*, 47-53. 10.1016/j.jncc.2024.01.006.
4. Miller, K.D., Nogueira, L., Devasia, T., et al. (2022). Cancer treatment and survivorship statistics, 2022. CA Cancer J Clin *72*, 409-436. 10.3322/caac.21731.
5. Nishida, C. and Yatera, K. (2022). The Impact of Ambient Environmental and Occupational Pollution on Respiratory Diseases. Int J Environ Res Public Health *19*. 10.3390/ijerph19052788.
6. Wang, Y., Bian, T., Song, L., et al. (2022). Reducing Chemotherapy-Induced DNA Damage via nAChR-Mediated Redox Reprograming-A New Mechanism for SCLC Chemoresistance Boosted by Nicotine. Cancers (Basel) *14*. 10.3390/cancers14092272.
7. Guglielmi, G. (2022). Almost half of cancer deaths are preventable. Nature. 10.1038/d41586-022-02355-x.
8. Hirsch, F.R., Scagliotti, G.V., Mulshine, J.L., et al. (2017). Lung cancer: current therapies and new targeted treatments. Lancet *389*, 299-311. 10.1016/s0140-6736(16)30958-8.

9. Hecht, S.S. (2002). Cigarette smoking and lung cancer: chemical mechanisms and approaches to prevention. Lancet Oncol *3*, 461-9. 10.1016/s1470-2045(02)00815-x.
10. Cheng, W.L., Chen, K.Y., Lee, K.Y., et al. (2020). Nicotinic-nAChR signaling mediates drug resistance in lung cancer. J Cancer *11*, 1125-1140. 10.7150/jca.36359.
11. Ge, G.Z., Xu, T.R. and Chen, C. (2015). Tobacco carcinogen NNK-induced lung cancer animal models and associated carcinogenic mechanisms. Acta Biochim Biophys Sin (Shanghai) *47*, 477-87. 10.1093/abbs/gmv041.
12. Wang, Y., Narayanapillai, S., Hu, Q., et al. (2018). Contribution of Tobacco Use and 4-(Methylnitrosamino)-1-(3-pyridyl)-1-butanone to Three Methyl DNA Adducts in Urine. Chem Res Toxicol *31*, 836-838. 10.1021/acs.chemrestox.8b00155.
13. Lou, Y., Guo, Z., Zhu, Y., et al. (2019). Houttuynia cordata Thunb. and its bioactive compound 2-undecanone significantly suppress benzo(a)pyrene-induced lung tumorigenesis by activating the Nrf2-HO-1/NQO-1 signaling pathway. J Exp Clin Cancer Res *38*, 242. 10.1186/s13046-019-1255-3.
14. Apel, K. and Hirt, H. (2004). Reactive oxygen species: metabolism, oxidative stress, and signal transduction. Annu Rev Plant Biol *55*, 373-99. 10.1146/annurev.arplant.55.031903.141701.
15. Ma, Q. (2013). Role of nrf2 in oxidative stress and toxicity. Annu Rev Pharmacol Toxicol *53*, 401-26. 10.1146/annurev-pharmtox-011112-140320.
16. Nath, M. and Agarwal, A. (2020). New insights into the role of heme oxygenase-1 in acute kidney injury. Kidney Res Clin Pract *39*, 387-401. 10.23876/j.krcp.20.091.
17. Thimmulappa, R.K., Rangasamy, T., Alam, J., et al. (2008). Dibenzoylmethane activates Nrf2-dependent detoxification pathway and inhibits benzo(a)pyrene induced DNA adducts in lungs. Med Chem *4*, 473-81. 10.2174/157340608785700199.
18. Mohamed, A.F., Safar, M.M., Zaki, H.F., et al. (2017). Telluric Acid Ameliorates Endotoxemic Kidney Injury in Mice: Involvement of TLR4, Nrf2, and PI3K/Akt Signaling Pathways. Inflammation *40*, 1742-1752. 10.1007/s10753-017-0617-2.
19. Schabbauer, G., Tencati, M., Pedersen, B., et al. (2004). PI3K-Akt pathway suppresses coagulation and inflammation in endotoxemic mice. Arterioscler Thromb Vasc Biol *24*, 1963-9. 10.1161/01.ATV.0000143096.15099.ce.
20. Bade, B.C. and Dela Cruz, C.S. (2020). Lung Cancer 2020: Epidemiology, Etiology, and Prevention. Clin Chest Med *41*, 1-24. 10.1016/j.ccm.2019.10.001.
21. de Groot, P.M., Wu, C.C., Carter, B.W., et al. (2018). The epidemiology of lung cancer. Transl Lung Cancer Res *7*, 220-233. 10.21037/tlcr.2018.05.06.
22. Liskova, A., Stefanicka, P., Samec, M., et al. (2020). Dietary phytochemicals as the potential protectors against carcinogenesis and their role in cancer chemoprevention. Clin Exp Med *20*, 173-190. 10.1007/s10238-020-00611-w.
23. Freeman, B., Mamallapalli, J., Bian, T., et al. (2023). Opportunities and Challenges of Kava in Lung Cancer Prevention. Int J Mol Sci *24*. 10.3390/ijms24119539.
24. Johnson, T.E., Hermanson, D., Wang, L., et al. (2011). Lung tumorigenesis suppressing effects of a commercial kava extract and its selected compounds in A/J mice. Am J Chin Med *39*, 727-42. 10.1142/s0192415x11009202.
25. Leitzman, P., Narayanapillai, S.C., Balbo, S., et al. (2014). Kava blocks 4-(methylnitrosamino)-1-(3-pyridyl)-1-butanone-induced lung tumorigenesis in association with reducing O6-methylguanine DNA adduct in A/J mice. Cancer Prev Res (Phila) *7*, 86-96. 10.1158/1940-6207.Capr-13-0301.
26. Narayanapillai, S.C., Balbo, S., Leitzman, P., et al. (2014). Dihydromethysticin from kava blocks tobacco carcinogen 4-(methylnitrosamino)-1-(3-pyridyl)-1-butanone-induced lung tumorigenesis and differentially reduces DNA damage in A/J mice. Carcinogenesis *35*, 2365-72. 10.1093/carcin/bgu149.
27. Johnson, T.E., Kassie, F., O'Sullivan, M.G., et al. (2008). Chemopreventive effect of kava on 4-(methylnitrosamino)-1-(3-pyridyl)-1-butanone plus benzo[a]pyrene-induced lung tumorigenesis in A/J mice. Cancer Prev Res (Phila) *1*, 430-8. 10.1158/1940-6207.Capr-08-0027.
28. Narayanapillai, S.C., Lin, S.H., Leitzman, P., et al. (2016). Dihydromethysticin (DHM) Blocks Tobacco Carcinogen 4-(Methylnitrosamino)-1-(3-pyridyl)-1-butanone (NNK)-Induced O(6)-Methylguanine in a Manner Independent of the Aryl Hydrocarbon Receptor (AhR) Pathway in C57BL/6 Female Mice. Chem Res Toxicol *29*, 1828-1834. 10.1021/acs.chemrestox.6b00203.

29. El-Saber Batiha, G., Magdy Beshbishy, A., L, G.W., et al. (2020). Chemical Constituents and Pharmacological Activities of Garlic (Allium sativum L.): A Review. Nutrients *12*. 10.3390/nu12030872.
30. Hall, A., Troupin, A., Londono-Renteria, B., et al. (2017). Garlic Organosulfur Compounds Reduce Inflammation and Oxidative Stress during Dengue Virus Infection. Viruses *9*. 10.3390/v9070159.
31. Zhang, L., Qu, Z., Song, A., et al. (2021). Garlic oil blocks tobacco carcinogen 4-(methylnitrosamino)-1-(3-pyridyl)-1-butanone (NNK)-induced lung tumorigenesis by inducing phase II drug-metabolizing enzymes. Food Chem Toxicol *157*, 112581. 10.1016/j.fct.2021.112581.
32. He, H., Ma, Y., Huang, H., et al. (2021). A comprehensive understanding about the pharmacological effect of diallyl disulfide other than its anti-carcinogenic activities. Eur J Pharmacol *893*, 173803. 10.1016/j.ejphar.2020.173803.
33. Tian, J., Zhao, W., Wu, Y., et al. (2023). Diallyl Disulfide Blocks Cigarette Carcinogen 4-(Methylnitrosamino)-1-(3-pyridyl)-1-butanone-Induced Lung Tumorigenesis via Activation of the Nrf2 Antioxidant System and Suppression of NF-κB Inflammatory Response. Journal of Agricultural and Food Chemistry *71*, 17763-17774. 10.1021/acs.jafc.3c02007.
34. Jiang, X., Zhu, X., Liu, N., et al. (2017). Diallyl Trisulfide Inhibits Growth of NCI-H460 in Vitro and in Vivo, and Ameliorates Cisplatin-Induced Oxidative Injury in the Treatment of Lung Carcinoma in Xenograft Mice. Int J Biol Sci *13*, 167-178. 10.7150/ijbs.16828.
35. Qu, Z., Tian, J., Sun, J., et al. (2024). Diallyl trisulfide inhibits 4-(methylnitrosamino)-1-(3-pyridyl)-1-butanone-induced lung cancer via modulating gut microbiota and the PPARγ/NF-κB pathway. Food & Function *15*, 158-171. 10.1039/d3fo03914e.
36. Kordiak, J., Bielec, F., Jabłoński, S., et al. (2022). Role of Beta-Carotene in Lung Cancer Primary Chemoprevention: A Systematic Review with Meta-Analysis and Meta-Regression. Nutrients *14*. 10.3390/nu14071361.
37. Xie, C., Zhou, X., Chen, W., et al. (2024). Diallyl trisulfide induces pyroptosis and impairs lung CSC-like properties by activating the ROS/Caspase 1 signaling pathway. Chem Biol Interact *397*, 111083. 10.1016/j.cbi.2024.111083.
38. Xiao, D., Zeng, Y., Hahm, E.R., et al. (2009). Diallyl trisulfide selectively causes Bax- and Bak-mediated apoptosis in human lung cancer cells. Environ Mol Mutagen *50*, 201-12. 10.1002/em.20431.
39. Li, Z., Feiyue, Z. and Gaofeng, L. (2021). Traditional Chinese medicine and lung cancer--From theory to practice. Biomed Pharmacother *137*, 111381. 10.1016/j.biopha.2021.111381.
40. Tian, W., Huang, J., Zhang, W., et al. (2024). Harnessing natural product polysaccharides against lung cancer and revisit its novel mechanism. Pharmacol Res *199*, 107034. 10.1016/j.phrs.2023.107034.
41. Chen, P., Wu, Q., Feng, J., et al. (2020). Erianin, a novel dibenzyl compound in Dendrobium extract, inhibits lung cancer cell growth and migration via calcium/calmodulin-dependent ferroptosis. Signal Transduct Target Ther *5*, 51. 10.1038/s41392-020-0149-3.
42. Hong, Y.S., Ham, Y.A., Choi, J.H., et al. (2000). Effects of allyl sulfur compounds and garlic extract on the expression of Bcl-2, Bax, and p53 in non small cell lung cancer cell lines. Exp Mol Med *32*, 127-34. 10.1038/emm.2000.22.
43. Goddard, K.A.B., Feuer, E.J., Mandelblatt, J.S., et al. (2025). Estimation of Cancer Deaths Averted From Prevention, Screening, and Treatment Efforts, 1975-2020. JAMA Oncol *11*, 162-167. 10.1001/jamaoncol.2024.5381.
44. Stinn, W., Teredesai, A., Kuhl, P., et al. (2005). Mechanisms involved in A/J mouse lung tumorigenesis induced by inhalation of an environmental tobacco smoke surrogate. Inhal Toxicol *17*, 263-76. 10.1080/08958370590922544.
45. Sødring, M., Gunnes, G. and Paulsen, J.E. (2016). Spontaneous initiation, promotion and progression of colorectal cancer in the novel A/J Min/+ mouse. Int J Cancer *138*, 1936-46. 10.1002/ijc.29928.
46. Han, Q., Fernandez, J., Rajczewski, A.T., et al. (2024). A Multi-Omics Study of Epigenetic Changes in Type II Alveolar Cells of A/J Mice Exposed to Environmental Tobacco Smoke. Int J Mol Sci *25*. 10.3390/ijms25179365.
47. Wang, H., Guo, L., Liu, F., et al. (2023). Brain distribution and metabolic profiling of 4-(methylnitrosamino)-1-(3-pyridyl)-1-butanone in rats investigated by UHPLC-HRMS/MS following peripheral administration. Anal Bioanal Chem *415*, 2317-2327. 10.1007/s00216-023-04655-1.
48. Chao, M.R., Cooke, M.S., Kuo, C.Y., et al. (2018). Children are particularly vulnerable to environmental tobacco smoke exposure: Evidence from biomarkers of tobacco-specific nitrosamines, and oxidative stress. Environ Int *120*, 238-245. 10.1016/j.envint.2018.08.006.

49. Bhagwat, S.V., Vijayasarathy, C., Raza, H., et al. (1998). Preferential effects of nicotine and 4-(N-methyl-N-nitrosamine)-1-(3-pyridyl)-1-butanone on mitochondrial glutathione S-transferase A4-4 induction and increased oxidative stress in the rat brain. Biochem Pharmacol *56*, 831-9. 10.1016/s0006-2952(98)00228-7.
50. Yang, B., Wang, G., Li, Y., et al. (2023). Hydroxycitric acid prevents hyperoxaluric-induced nephrolithiasis and oxidative stress via activation of the Nrf2/Keap1 signaling pathway. Cell Cycle *22*, 1884-1899. 10.1080/15384101.2023.2247251.
51. Zhang, S., Duan, S., Xie, Z., et al. (2022). Epigenetic Therapeutics Targeting NRF2/KEAP1 Signaling in Cancer Oxidative Stress. Front Pharmacol *13*, 924817. 10.3389/fphar.2022.924817.
52. Kumari, S., Badana, A.K., G, M.M., et al. (2018). Reactive Oxygen Species: A Key Constituent in Cancer Survival. Biomark Insights *13*, 1177271918755391. 10.1177/1177271918755391.
53. Morgenstern, C., Lastres-Becker, I., Demirdöğen, B.C., et al. (2024). Biomarkers of NRF2 signalling: Current status and future challenges. Redox Biol *72*, 103134. 10.1016/j.redox.2024.103134.
54. Fan, Z., Wirth, A.K., Chen, D., et al. (2017). Nrf2-Keap1 pathway promotes cell proliferation and diminishes ferroptosis. Oncogenesis *6*, e371. 10.1038/oncsis.2017.65.
55. Alzain, A.A., Mukhtar, R.M., Abdelmoniem, N., et al. (2023). Modulation of NRF2/KEAP1-Mediated Oxidative Stress for Cancer Treatment by Natural Products Using Pharmacophore-Based Screening, Molecular Docking, and Molecular Dynamics Studies. Molecules *28*. 10.3390/molecules28166003.
56. Zhang, H., Liu, H., Davies, K.J., et al. (2012). Nrf2-regulated phase II enzymes are induced by chronic ambient nanoparticle exposure in young mice with age-related impairments. Free Radic Biol Med *52*, 2038-46. 10.1016/j.freeradbiomed.2012.02.042.
57. Kumar, B., Koul, S., Khandrika, L., et al. (2008). Oxidative stress is inherent in prostate cancer cells and is required for aggressive phenotype. Cancer Res *68*, 1777-85. 10.1158/0008-5472.Can-07-5259.
58. Slocum, S.L. and Kensler, T.W. (2011). Nrf2: control of sensitivity to carcinogens. Arch Toxicol *85*, 273-84. 10.1007/s00204-011-0675-4.
59. Yang, Y., Yang, Y., Huang, H., et al. (2023). PLCG2 can exist in eccDNA and contribute to the metastasis of non-small cell lung cancer by regulating mitochondrial respiration. Cell Death Dis *14*, 257. 10.1038/s41419-023-05755-7.
60. Martinez Molina, D., Jafari, R., Ignatushchenko, M., et al. (2013). Monitoring drug target engagement in cells and tissues using the cellular thermal shift assay. Science *341*, 84-7. 10.1126/science.1233606.
61. Hu, X., Gan, L., Tang, Z., et al. (2024). A Natural Small Molecule Mitigates Kidney Fibrosis by Targeting Cdc42-mediated GSK-3β/β-catenin Signaling. Adv Sci (Weinh) *11*, e2307850. 10.1002/advs.202307850.
62. Xu, S., Chen, Y., Miao, J., et al. (2024). Esculin inhibits hepatic stellate cell activation and CCl(4)-induced liver fibrosis by activating the Nrf2/GPX4 signaling pathway. Phytomedicine *128*, 155465. 10.1016/j.phymed.2024.155465.
63. Qu, Z., Tian, J., Sun, J., et al. (2024). Diallyl trisulfide inhibits 4-(methylnitrosamino)-1-(3-pyridyl)-1-butanone-induced lung cancer via modulating gut microbiota and the PPARγ/NF-κB pathway. Food Funct *15*, 158-171. 10.1039/d3fo03914e.
64. Ferguson, D.T., Taka, E., Messeha, S., et al. (2024). The Garlic Compound, Diallyl Trisulfide, Attenuates Benzo[a]Pyrene-Induced Precancerous Effect through Its Antioxidant Effect, AhR Inhibition, and Increased DNA Repair in Human Breast Epithelial Cells. Nutrients *16*. 10.3390/nu16020300.
65. Suzuki, T., Shibata, T., Takaya, K., et al. (2013). Regulatory nexus of synthesis and degradation deciphers cellular Nrf2 expression levels. Mol Cell Biol *33*, 2402-12. 10.1128/mcb.00065-13.
66. Nagae, S., Ushijima, M., Hatono, S., et al. (1994). Pharmacokinetics of the garlic compound S-allylcysteine. Planta Med *60*, 214-7. 10.1055/s-2006-959461.
67. Lawson, L.D. and Wang, Z.J. (2005). Allicin and allicin-derived garlic compounds increase breath acetone through allyl methyl sulfide: use in measuring allicin bioavailability. J Agric Food Chem *53*, 1974-83. 10.1021/jf048323s.
68. Rojo, A.I., Rada, P., Mendiola, M., et al. (2014). The PTEN/NRF2 axis promotes human carcinogenesis. Antioxid Redox Signal *21*, 2498-514. 10.1089/ars.2014.5843.
69. Sporn, M.B. and Liby, K.T. (2012). NRF2 and cancer: the good, the bad and the importance of context. Nat Rev Cancer *12*, 564-71. 10.1038/nrc3278.